chemistry

MDPI

Article

The Impact of Structural Defects on Iodine Adsorption in UiO-66

John Maddock [1], Xinchen Kang [1], Lifei Liu [2], Buxing Han [2], Sihai Yang [1,*] and Martin Schröder [1,*]

[1] Department of Chemistry, University of Manchester, Manchester M13 9PL, UK; john.maddock@manchester.ac.uk (J.M.); kangxinchen@iccas.ac.cn (X.K.)
[2] Beijing National Laboratory for Molecular Sciences, CAS Key Laboratory of Colloid, Interface and Chemical Thermodynamics, Institute of Chemistry, Chinese Academy of Science, Beijing 100190, China; liulifei@iccas.ac.cn (L.L.); hanbx@iccas.ac.cn (B.H.)
* Correspondence: sihai.yang@manchester.ac.uk (S.Y.); M.Schroder@manchester.ac.uk (M.S.); Tel.: +44-161-275-1066 (S.Y.); +44-161-306-9119 (M.S.)

Abstract: Radioactive I_2 (iodine) produced as a by-product of nuclear fission poses a risk to public health if released into the environment, and it is thus vital to develop materials that can capture I_2 vapour. Materials designed for the capture and storage of I_2 must have a high uptake capacity and be stable for long-term storage due the long half-life of ^{129}I. UiO-66 is a highly stable and readily tuneable metal-organic framework (MOF) into which defect sites can be introduced. Here, a defective form of UiO-66 (UiO-66-FA) was synthesised and the presence of missing cluster moieties confirmed using confocal fluorescence microscopy and gas sorption measurements. The uptake of I_2 vapour in UiO-66-FA was measured using thermal gravimetric analysis coupled mass spectrometry (TGA-MS) to be 2.25 g g^{-1}, almost twice that (1.17 g g^{-1}) of the pristine UiO-66. This study will inspire the design of new efficient I_2 stores based upon MOFs incorporating structural defects.

Keywords: metal organic frameworks; defect; iodine adsorption; UiO-66

Citation: Maddock, J.; Kang, X.; Liu, L.; Han, B.; Yang, S.; Schröder, M. The Impact of Structural Defects on Iodine Adsorption in UiO-66. *Chemistry* **2021**, *3*, 525–531. https://doi.org/10.3390/chemistry3020037

Academic Editor: Catherine Housecroft

Received: 1 March 2021
Accepted: 8 April 2021
Published: 12 April 2021

1. Introduction

Nuclear power is responsible for approximately 21% of the UK's energy production as of 2020 [1]. The products produced as a result of the fission of uranium pose a danger to the environment and public health, and so materials that can capture and store such fission products are of significant interest. ^{131}I and ^{129}I are volatile fission products with half-lives of 8 days and 1.57×10^7 years, respectively [2]. ^{131}I poses a serious risk to human health as it has been linked to the occurrence of thyroid cancer [3]. ^{129}I is less hazardous due to its low energy beta and gamma emissions, but poses a long-term environmental risk due to bioaccumulation [4]. It is vital also to prevent I_2 escaping into the environment as it can spread over a wide area due to its high solubility in water [5]. The capture of I_2 has been investigated using a wide variety of porous materials such as aerogels [6], zeolites [7], porous organic polymers [8] and covalent–organic framework [9] materials. The main drawbacks to using these materials are that they can be non-specific for I_2, have low uptakes, or have amorphous structures that prevent determination of preferred binding sites, thus restricting an understanding of the mechanism of action of the material.

Metal–organic framework (MOF) materials are often highly porous and crystalline and are well-known for their tuneable structures, potential high chemical stability and high surface areas [10]. The tunability of MOFs has allowed them to be used in a wide range of applications including catalysis [11], molecular separations [12] and the capture of gases such as CO_2 [13] and SO_2 [14]. The storage of I_2 by MOFs has been reported previously with uptakes reaching as high as 7.35 g g^{-1} in the case of the ionic liquid-doped material PCN-333 [15]. Proof-of-concept studies have also shown that MOFs can be used for the long-term storage of I_2 using glass sintering [16] and pressure-induced amorphization [17].

Functionalisation of the MOF structure is a common route to increasing I_2 adsorption and relies on the introduction of electron donating [18,19] or reactive groups [20] onto the ligands. Doping MOFs with Ag [21] and Cu [22] ions can also improve the I_2 uptake of the host MOF. Detailed studies into the adsorption mechanism of I_2 have also been carried out and highlight the importance of the structure of the MOF [23,24] and of metal cluster nodes for the efficient capture of I_2 [25]. The introduction of structural defects has been shown to increase the catalytic activity of MOFs [26,27] and increase the uptake of CO_2 by UiO-66 [28]. However, the impact of such defects on the adsorption of I_2 has not been investigated previously and we were interested to determine whether this was an appropriate methodology for improved I_2 adsorption (Figure S1, Supplementary Materials).

UiO-66 was chosen in this work due its high stability and the established synthesis and routes to the preparation of defective derivatives. Coordination modulation by undertaking the synthesis of UiO-66 in the presence of formic acid can introduce defects into UiO-66. The competitor ligand formate binds to metal clusters in place of the bridging terephthalate linker to produce missing linker defects. If there is sufficient missing linker, defects will occur within the overall stable geometry with certain metal clusters absent (Figure S2) [29]. We have analysed the presence of missing cluster defects within a sample of defect UiO-66, designated UiO-66-FA, using Brunauer–Emmett–Teller (BET) surface area analysis, thermal gravimetric analysis and confocal fluorescence microscopy. The uptake of I_2 has been measured and confirmed using Raman spectroscopy and thermal gravimetric analysis coupled with mass spectrometry. The presence of structural defects results in a nearly 100% enhancement in the adsorption capacity of I_2 within UiO-66-FA compared to pristine UiO-66.

2. Results and Discussion

UiO-66 was synthesised by dissolving $ZrCl_4$ and terephthalic acid in DMF and heating the solution to 120 °C for 24 h. UiO-66-FA was synthesised using the same general procedure but using a mixture of DMF and formic acid as solvent. Powder X-ray diffraction (PXRD) analysis of as-synthesised UiO-66 and UiO-66-FA (Figure 1) confirmed the phase purity of both samples [30,31]. The PXRD pattern of UiO-66-FA shows two additional Bragg peaks between 5 and 7° attributed to the presence of *reo* regions within the *fcu* structure caused by missing cluster defects [29,32]. These Bragg peaks are also broad, highlighting the disorder of these defect sites throughout the parent structure of UiO-66.

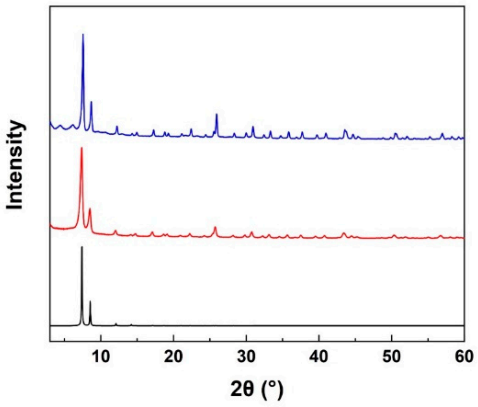

Figure 1. PXRD (powder X-ray diffraction) patterns for UiO-66 synthesised with (blue) and without formic acid (red). Simulated PXRD for UiO-66 (black) [27].

Confocal fluorescence microscopy (CFM) can be used to visualise mesoporous defects within electro-synthesised MOFs [27]. In these systems, Lewis acid sites found in defect sites and boundaries catalyse the formation of a fluorescent oligomer from furfuryl alcohol, the monomer of which is not fluorescent (Figure S3). On exposure of UiO-66 and UiO-66-FA to furfuryl alcohol it was noted that the UiO-66-FA sample had a darker colour

than the sample exposed to UiO-66 (Figure S4). This suggested that a more fluorescent oligomer was being produced by UiO-66-FA as the oligomer has a dark brown colour compared to the colourless furfuryl alcohol. This conclusion was supported by CFM which showed a uniform spread of high intensity fluorescence throughout the sample of UiO-66-FA exposed to furfuryl alcohol. The sample of UiO-66 exposed to furfuryl alcohol shows weaker fluorescence which is not evenly distributed across the sample (Figure 2). The relatively small amount of fluorescence and its location for the UiO-66 sample can be explained by the presence of Lewis acid sites at the edges of the crystals, with the high intensity fluorescence across the sample of UiO-66-FA confirming the presence of an increased number of defects within the structure of UiO-66-FA compared to UiO-66.

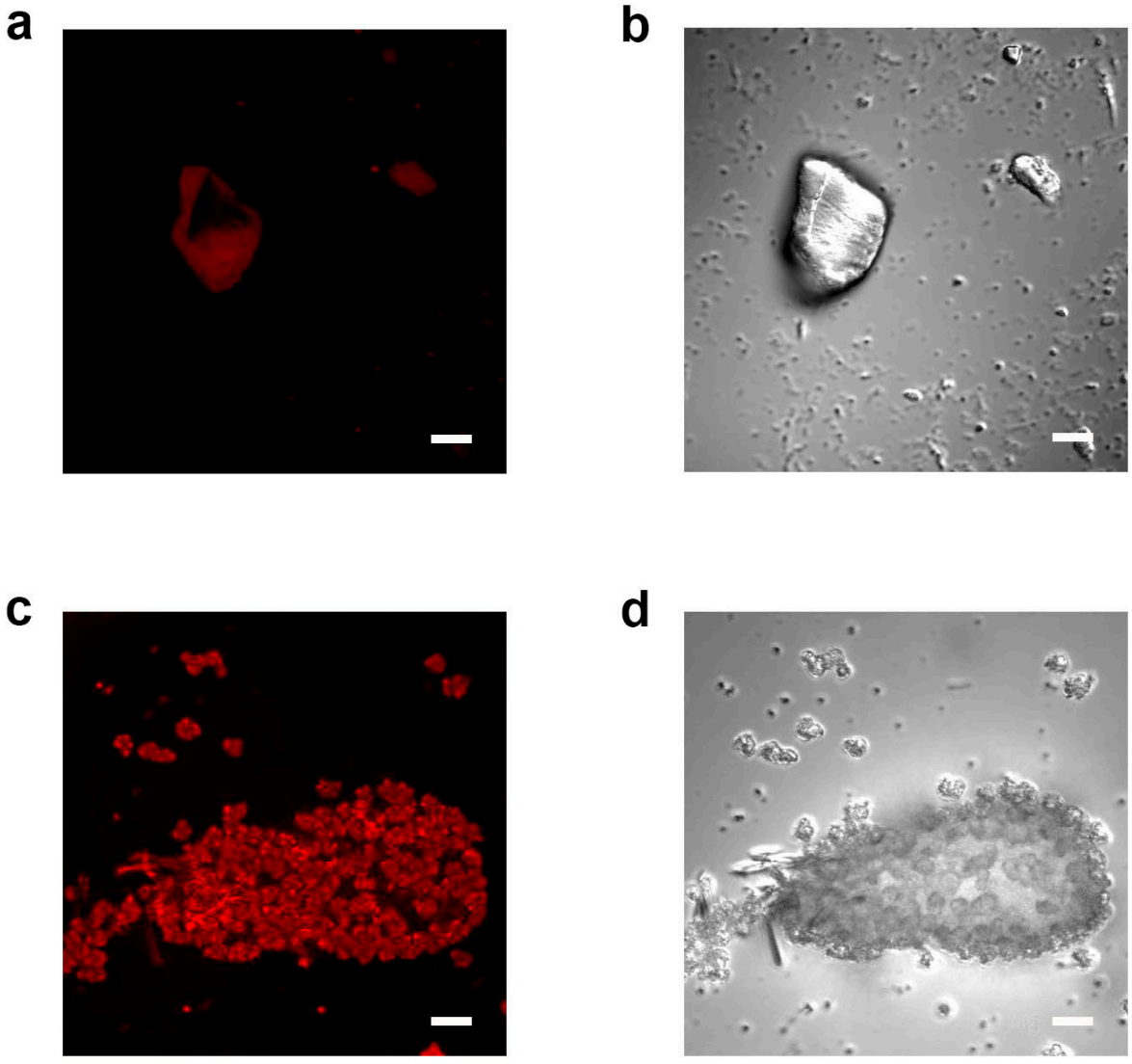

Figure 2. CFM (confocal fluorescence microscopy) and micrograph images: (**a**) fluorescence micrograph of UiO-66; (**b**) micrograph of UiO-66; (**c**) fluorescence micrograph of UiO-66-FA; (**d**) micrograph of UiO-66-FA. Scale bars are 10 μm, 10 μm, 5 μm and 5 μm, respectively.

UiO-66-FA shows a higher BET surface area than UiO-66, 1705 and 1170 m^2 g^{-1}, respectively, as determined from the N_2 adsorption isotherm, consistent with the removal of linkers and clusters to form defect sites in UiO-66-FA. The pore size distribution data (Figure S5) confirm that larger pores are present in UiO-66-FA with significant peaks above 8 Å radius attributed to the large pores created due to missing cluster moieties. In contrast, UiO-66 only shows pores of less than 9 Å radius [30]. The calculated micropore volume

also supports the formation of larger pores with 0.30 cm^3 g^{-1} in UiO-66 and 0.73 cm^3 g^{-1} in UiO-66-FA. PXRD, CFM and BET results confirm the presence of defects in UiO-66-FA.

I_2 adsorption was carried out in a sealed flask by heating for 3 days the activated, desolvated solid MOF sample with solid I_2, each inside an open glass vessel. The MOF sample was then removed from the vessel for further analysis. TGA analysis of the I_2-loaded samples showed a drop in mass between 100 and 200 °C attributed to loss of I_2 as monitored by mass spectrometry (Figure 3). The I_2 uptake over three repeat cycles gave an average uptake for UiO-66 and UiO-66-FA of 1.17 and 2.25 g g^{-1}, respectively, consistent with the increased porosity due to defects in the structure of UiO-66-FA. The weight drop observed at around 500 °C is linked to decomposition of the ligand and the percentage drop for UiO-66-FA is less than that of UiO-66, reflecting fewer ligands present in the UiO-66-FA. The Raman spectrum of solid I_2 shows a peak at 180 cm^{-1} assigned to the υI-I stretching vibration. This peak is shifted in both I_2-loaded UiO-66 samples (Figure 4), and the presence of this single peak rules out the presence of triiodide that would produce a peak between 110 and 140 cm^{-1} [33]. Other observable features in the complete Raman spectra (Figure S6) include peaks at 1600 cm^{-1}, 1150 cm^{-1} and 850 cm^{-1} assigned to the C-C bonds in the aromatic ring of the ligand [34]. The overlapping peaks seen at 1400 cm^{-1} are due to the COO stretching vibration of the linker overlapping with another aromatic ring Raman peak. There is no change to these peaks upon I_2 adsorption in both UiO-66 and UiO-66-FA, confirming that the linker remains intact after I_2 adsorption. I_2 has strong interaction with unsaturated zirconium clusters and increased access to the framework of UiO-66-FA results in a high I_2 uptake.

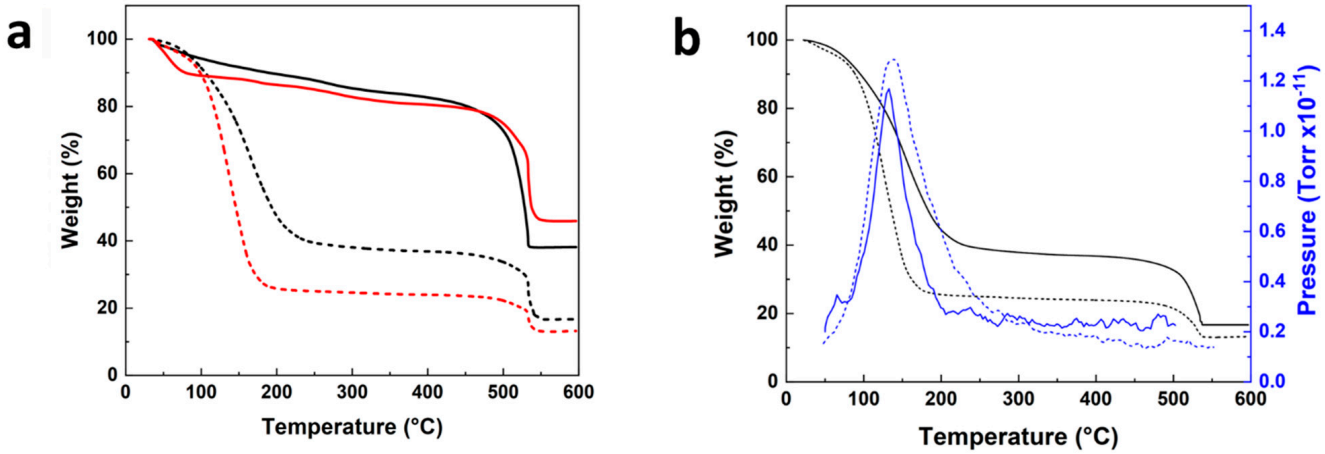

Figure 3. (**a**) TGA for UiO-66 (black) and UiO-66-FA (red); dashed lines indicate I_2-loaded samples. (**b**) TGA-MS results (black line) for I_2-loaded UiO-66 (solid line) and I_2-loaded UiO-66-FA (dashed).

The cycling of I_2 adsorption was carried out to show that even when clusters are removed from UiO-66 the structure remains stable on the adsorption and desorption of I_2 (Figure 5). The decrease in I_2 uptake observed after each cycle in derivatives of UiO-66 has been observed previously [25,35]. However, this drop in uptake appears to be less for UiO-66-FA, which could be due to the openness of the structure reducing the impact of I_2 removal. Samples of MOF were monitored by PXRD on removal of I_2 from loaded material (Figures S7 and S8). The PXRD patterns show little change in the structure or crystallinity throughout the cycling experiments, confirming that defects within UiO-66-FA do not decrease its stability on I_2 loading.

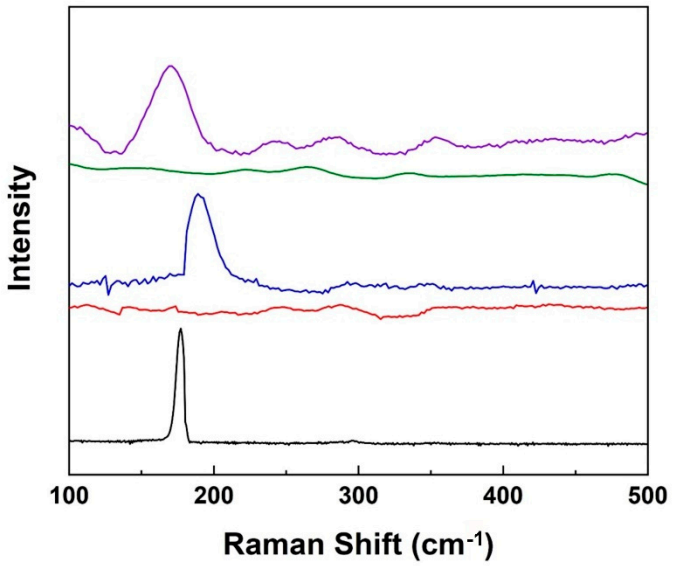

Figure 4. Raman spectra of solid I_2 (black), activated UiO-66 (blue), I_2-loaded UiO-66 (red), activated UiO-66-FA (green) and I_2-loaded UiO-66-FA (purple). The complete spectra are shown in Figure S5.

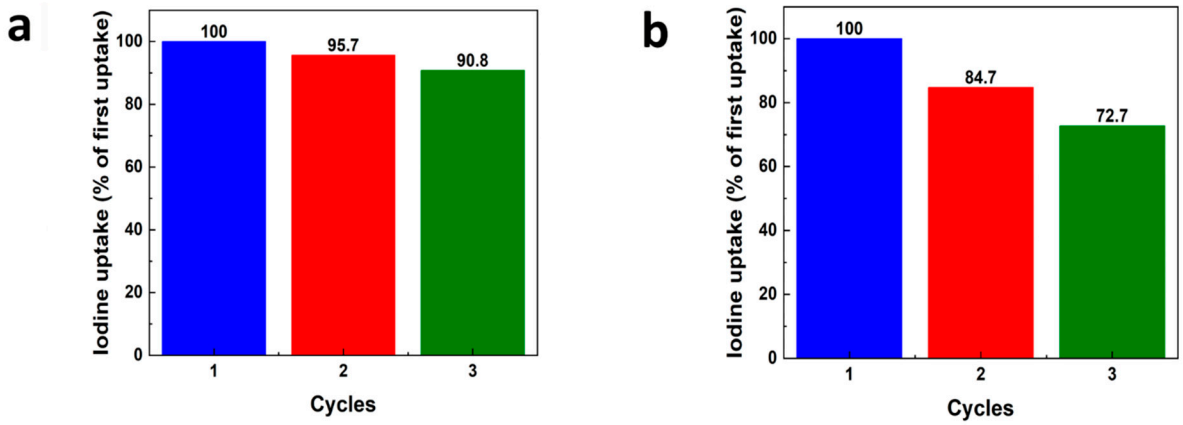

Figure 5. I_2 uptakes compared to the first cycle for (**a**) UiO-66 and (**b**) UiO-66-FA. First cycle (blue), second cycle (red) and third cycle (green). PXRD of samples after I_2 desorption are shown in Figures S7 and S8.

In summary, the impact of structural defects on I_2 uptake capacity has been studied in UiO-66 and UiO-66-FA. The presence of defects in UiO-66-FA was verified by BET surface area, TGA and CFM analysis. Defects caused by missing clusters within the structure of UiO-66 results in an increase I_2 adsorption from 1.17 to 2.25 g g^{-1} for UiO-66 and UiO-66-FA, respectively, and the overall increased porosity of the latter also contributes to higher I_2 uptake. Cycling of I_2 loading in UiO-66-FA confirms that I_2 uptake can be increased without compromising the stability of the MOF, an approach that can be applied potentially to other capture systems.

Supplementary Materials: The following are available online at https://www.mdpi.com/article/10.3390/chemistry3020037/s1, Figure S1: Colour change observed in UiO-66-FA with loading of I_2. Figure S2: Structure of UiO-66 and of UiO-66-FA. Figure S3: Reaction scheme for the synthesis of the fluorescent oligomer from furfuryl alcohol. Figure S4: Sample of UiO-66 and UiO-66-FA in furfuryl alcohol after oligomerization reaction. Figure S5: N_2 adsorption isotherm and pore size distribution of UiO-66 and UiO-66-FA. Figure S6: Raman spectra of I_2, UiO-66, I_2-loaded UiO-66, UiO-66-FA, and I_2-loaded UiO-66-FA. Figure S7: PXRD of UiO-66 after removal of captured I_2. Figure S8: PXRD of UiO-66-FA after removal of captured I_2.

Author Contributions: J.M. and X.K.: all experimental work; J.M. and L.L.: validation experiments; B.H., S.Y. and M.S.: design of project, supervision and overall strategy of project. All authors have contributed to the preparation of the manuscript. All authors have read and agreed to the published version of the manuscript.

Funding: We thank EPSRC (EP/I011870) and the Royal Society (IC170327), National Natural Science Foundation of China (21733011, 21890761), the University of Manchester and Institute of Chemistry, Chinese Academy of Sciences for funding. This project has received funding from the European Research Council (ERC) under the European Union's Horizon 2020 research and innovation programme (grant agreement No 742401, *NANOCHEM*). X.K. is supported by Royal Society Newton International Fellowship.

Conflicts of Interest: The authors declare no conflict of interest.

References

1. World Nuclear Association. Nuclear Power in the United Kingdom. Available online: https://www.world-nuclear.org/information-library/country-profiles/countries-t-z/united-kingdom.aspx (accessed on 27 June 2020).
2. Audi, G.; Bersillon, O.; Blachot, J.; Wapstra, A.H. The NUBASE evaluation of nuclear and decay properties. *Nucl. Phys. A* **2003**, *729*, 3–128. [CrossRef]
3. Shakhtarin, V.V.; Tsyb, A.F.; Stepanenko, V.F.; Orlov, M.Y.; Kopecky, K.J.; Davis, S. Iodine deficiency, radiation dose, and the risk of thyroid cancer among children and adolescents in the Bryansk region of Russia following the Chernobyl power station accident. *Int. J. Epidemiol.* **2003**, *32*, 584–591. [CrossRef]
4. Satoh, Y.; Ueda, S.; Kakiuchi, H.; Ohtsuka, Y.; Hisamatsu, S.J. Concentrations of iodine-129 in coastal surface sediments around spent nuclear fuel reprocessing plant at Rokkasho, Japan, during and after its test operation. *Radioanal. Nucl. Chem.* **2019**, *322*, 2019–2024. [CrossRef]
5. Ioannides, K.; Stamoulis, K.; Papachristodoulou, C.J. Environmental radioactivity measurements in north–western Greece following the Fukushima nuclear accident. *Radioanal. Nucl. Chem.* **2013**, *298*, 1207–1213. [CrossRef]
6. Riley, B.J.; Chun, J.; Ryan, J.V.; Matyáš, J.; Li, X.S.; Matson, D.W.; Sundaram, S.K.; Strachan, D.M.; Vienna, J.D. Chalcogen-based aerogels as a multifunctional platform for remediation of radioactive iodine. *RSC Adv.* **2011**, *1*, 1704–1715. [CrossRef]
7. Chibani, S.; Chebbi, M.; Lebègue, S.; Cantrel, L.; Badawi, M. Impact of the Si/Al ratio on the selective capture of iodine compounds in silver-mordenite: A periodic DFT study. *Phys. Chem. Chem. Phys.* **2016**, *18*, 25574–25581. [CrossRef]
8. Su, K.; Wang, W.; Li, B.; Yuan, D. Azo-bridged calix[4]resorcinarene-based porous organic frameworks with highly efficient enrichment of volatile iodine. *ACS Sustain. Chem. Eng.* **2018**, *6*, 17402–17409. [CrossRef]
9. Wang, C.; Wang, Y.; Ge, R.; Song, X.; Xing, X.; Jiang, Q.; Lu, H.; Hao, C.; Guo, X.; Gao, Y.; et al. A 3D covalent organic framework with exceptionally high iodine capture capability. *Chem. Eur. J.* **2018**, *24*, 585–589. [CrossRef]
10. Furukawa, H.; Cordova, K.E.; O'Keeffe, M.; Yaghi, O.M. The chemistry and applications of metal-organic frameworks. *Science* **2013**, *341*, 1230444. [CrossRef] [PubMed]
11. Caratelli, C.; Hajek, J.; Cirujano, F.G.; Waroquier, M.; Xamena, F.X.L.I.; van Speybroeck, V. Nature of active sites on UiO-66 and beneficial influence of water in the catalysis of Fischer esterification. *J. Catal.* **2017**, *352*, 401–414. [CrossRef]
12. Herm, Z.R.; Bloch, E.D.; Long, J.R. Hydrocarbon Separations in metal–organic frameworks. *Chem. Mater.* **2014**, *26*, 323–338. [CrossRef]
13. Ding, M.; Flaig, R.W.; Jiang, H.L.; Yaghi, O.M. Carbon capture and conversion using metal–organic frameworks and MOF-based materials. *Chem. Soc. Rev.* **2019**, *48*, 2783–2828. [CrossRef]
14. Smith, G.L.; Eyley, J.E.; Han, X.; Zhang, X.; Li, J.; Jacques, N.M.; Godfrey, H.G.W.; Argent, S.P.; McPherson, L.J.M.; Teat, S.J.; et al. Reversible coordinative binding and separation of sulfur dioxide in a robust metal–organic framework with open copper sites. *Nat. Mater.* **2019**, *18*, 1358–1365. [CrossRef]
15. Tang, Y.; Huang, H.; Li, J.; Xue, W.; Zhong, C. IL-induced formation of dynamic complex iodide anions in IL@MOF composites for efficient iodine capture. J. *Mater. Chem. A* **2019**, *7*, 18324–18329. [CrossRef]
16. Sava, D.F.; Garino, T.J.; Nenoff, T.M. Iodine confinement into metal–organic frameworks (mofs): Low-temperature sintering glasses to form novel glass composite material (GCM) alternative waste forms. *Ind. Eng. Chem. Res.* **2012**, *51*, 614–620. [CrossRef]
17. Chapman, K.W.; Sava, D.F.; Halder, G.J.; Chupas, P.J.; Nenoff, T.M. Trapping guests within a nanoporous metal-organic framework through pressure-induced amorphization. *J. Am. Chem. Soc.* **2011**, *133*, 18583–18585. [CrossRef] [PubMed]
18. Munn, A.S.; Millange, F.; Frigoli, M.; Guillou, N.; Falaise, C.; Stevenson, V.; Volkringer, C.; Loiseau, T.; Cibin, G.; Walton, R.I. Iodine sequestration by thiol-modified MIL-53(Al). *CrystEngComm* **2016**, *18*, 8108–8114. [CrossRef]
19. Falaise, C.; Volkringer, C.; Facqueur, J.; Bousquet, T.; Gasnot, L.; Loiseau, T. Capture of iodine in highly stable metal–organic frameworks: A systematic study. *Chem. Commun.* **2013**, *49*, 10320–10322. [CrossRef]
20. Marshall, R.J.; Griffin, S.L.; Wilson, C.; Forgan, R.S. Postsynthetic bromination of UiO-66 analogues: Altering linker flexibility and mechanical compliance. *Chem. Eur. J.* **2016**, *22*, 4870–4877. [CrossRef] [PubMed]
21. Chen, J.; Gao, Q.; Zhang, X.; Liu, Y.; Wang, P.; Jiao, Y.; Yang, Y. Nanometer mixed-valence silver oxide enhancing adsorption of ZIF-8 for removal of iodide in solution. *Sci. Total Environ.* **2019**, *646*, 634–644. [CrossRef]

22. Qi, B.; Liu, Y.; Zheng, T.; Gao, Q.; Yan, X.; Jiao, Y.; Yang, Y.J. Highly efficient capture of iodine by Cu/MIL-101. *Solid State Chem.* **2018**, *258*, 49–55. [CrossRef]
23. Zhang, X.; da Silva, I.; Godfrey, H.G.W.; Callear, S.K.; Sapchenko, S.A.; Cheng, Y.; Vitórica-Yrezábal, I.; Frogley, M.D.; Cinque, G.; Tang, C.C.; et al. Confinement of iodine molecules into triple-helical chains within robust metal–organic frameworks. *J. Am. Chem. Soc.* **2017**, *139*, 16289–16296. [CrossRef]
24. Gallis, D.F.S.; Ermanoski, I.; Greathouse, J.A.; Chapman, K.W.; Nenoff, T.M. Iodine gas adsorption in nanoporous materials: A combined experiment–modeling study. *Ind. Eng. Chem. Res.* **2017**, *56*, 2331–2338. [CrossRef]
25. Chen, P.; He, X.; Pang, M.; Dong, X.; Zhao, S.; Zhang, W. Iodine capture using Zr-based metal–organic frameworks (Zr-MOFs): Adsorption performance and mechanism. *ACS Appl. Mater. Interfaces* **2020**, *12*, 20429–20439. [CrossRef]
26. Chaemchuen, S.; Luo, Z.; Zhou, K.; Mousavi, B.; Phatanasri, S.; Jaroniec, M.; Verpoort, F. Defect formation in metal–organic frameworks initiated by the crystal growth-rate and effect on catalytic performance. *J. Catal.* **2017**, *354*, 84–91. [CrossRef]
27. Kang, X.; Lyu, K.; Li, L.; Li, J.; Kimberley, L.; Wang, B.; Liu, L.; Cheng, Y.; Frogley, M.D.; Rudić, S.; et al. Integration of mesopores and crystal defects in metal-organic frameworks via templated electrosynthesis. *Nat. Commun.* **2019**, *10*, 1–9. [CrossRef] [PubMed]
28. Wu, H.; Chua, Y.S.; Krungleviciute, V.; Tyagi, M.; Chen, P.; Yildirim, T.; Zhou, W. Unusual and highly tunable missing-linker defects in zirconium metal–organic framework UIO-66 and their important effects on gas adsorption. *J. Am. Chem. Soc.* **2013**, *135*, 10525–10532. [CrossRef]
29. Shearer, G.C.; Vitillo, J.G.; Bordiga, S.; Svelle, S.; Olsbye, U.; Lillerud, K.P. Functionalizing the defects: Postsynthetic ligand exchange in the metal organic framework UiO-66. *Chem. Mater.* **2016**, *28*, 7190–7193. [CrossRef]
30. Koutsianos, A.; Kazimierska, E.; Barron, A.R.; Taddei, M.; Andreoli, E. A new approach to enhancing the CO_2 capture performance of defective UiO-66 via post-synthetic defect exchange. *Dalton Trans.* **2019**, *48*, 3349–3359. [CrossRef]
31. Cavka, J.H.; Jakobsen, S.; Olsbye, U.; Guillou, N.; Lamberti, C.; Bordiga, S.; Lillerud, K.P. A new zirconium inorganic building brick forming metal organic frameworks with exceptional stability. *J. Am. Chem. Soc.* **2008**, *130*, 13850–13851. [CrossRef] [PubMed]
32. DeStefano, M.R.; Islamoglu, T.; Garibay, S.J.; Hupp, J.T.; Farha, O.K. Room-temperature synthesis of UiO-66 and thermal modulation of densities of defect sites. *Chem. Mater.* **2017**, *29*, 1357–1361. [CrossRef]
33. Svensson, P.H.; Kloo, L. Synthesis, structure, and bonding in polyiodide and metal iodide—iodine systems. *Chem. Rev.* **2003**, *103*, 1649–1684. [CrossRef] [PubMed]
34. Schwan, J.; Ulrich, S.; Batori, V.; Ehrhardt, H.; Silva, S.R.P. Raman spectroscopy on amorphous carbon films. *J. Appl. Phys.* **1996**, *80*, 440–447. [CrossRef]
35. Wang, Z.; Huang, Y.; Yang, J.; Li, Y.; Zhuang, Q.; Gu, J. The water-based synthesis of chemically stable Zr-based MOFs using pyridine-containing ligands and their exceptionally high adsorption capacity for iodine. *Dalton Trans.* **2017**, *46*, 7412–7420. [CrossRef] [PubMed]